COMPUTER METHODS AND PROGRAMS IN BIOMEDICINE 86 (2007) 232–244

journal homepage: www.intl.elsevierhealth.com/journals/cmpb

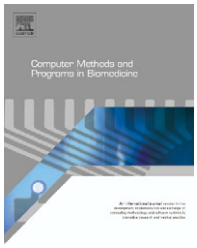

Computational models of myocardial endomysial collagen arrangement

Benedetto Intrigila[a], *Igor Melatti*[b], *Alberto Tofani*[c,*], *Guido Macchiarelli*[d]

[a] *Dip. di Matematica Pura ed Applicata, Università di Roma "Tor Vergata", 00133 Roma, Italy*
[b] *Dip. di Informatica, Università di Roma "La Sapienza", 00198 Roma, Italy*
[c] *Dip. di Informatica, Università di L'Aquila, Coppito 67100, L'Aquila, Italy*
[d] *Dip. di Medicina Sperimentale, Università di L'Aquila, Coppito 67100, L'Aquila, Italy*

ARTICLE INFO

Article history:
Received 28 July 2006
Received in revised form
17 November 2006
Accepted 9 March 2007

Keywords:
Collagen
Endomysium
Heart mechanics
Modelling
Neural networks
Scanning electron microscopy

ABSTRACT

Collagen extracellular matrix is one of the factors related to high passive stiffness of cardiac muscle. However, the architecture and the mechanical aspects of the cardiac collagen matrix are not completely known.

In particular, endomysial collagen contribution to the passive mechanics of cardiac muscle as well as its micro anatomical arrangement is still a matter of debate.

In order to investigate mechanical and structural properties of endomysial collagen, we consider two *alternative* computational models of some specific aspects of the cardiac muscle.

These two models represent two different views of endomysial collagen distribution: (1) the traditional view and (2) a new view suggested by the data obtained from scanning electron microscopy (SEM) in NaOH macerated samples (a method for isolating collagen from the other tissue).

We model the myocardial tissue as a net of spring elements representing the cardiomyocytes together with the endomysial collagen distribution. Each element is a viscous elastic spring, characterized by an elastic and a viscous constant. We connect these springs to imitate the interconnections between collagen fibers. Then we apply to the net of springs some external forces of suitable magnitude and direction, obtaining an extension of the net itself. In our setting, the ratio *forces magnitude /net extension* is intended to model the *stress /strain ratio* of a microscopical portion of the myocardial tissue.

To solve the problem of the correct identification of the values of the different parameters involved, we use an *artificial neural network* approach. In particular, we use this technique to *learn*, given a distribution of external forces, the elastic constants of the springs needed to obtain a desired extension as an equilibrium position.

Our experimental findings show that, in the model of collagen distribution structured according to the new view, a given *stress /strain ratio* (of the net of springs, in the sense specified above) is obtained with much smaller (w.r.t. the other model, corresponding to the traditional view) elasticity constants of the springs.

This seems to indicate that by an appropriate structure, a given *stiffness* of the myocardial tissue can be obtained with endomysial collagen fibers of much smaller size.

* *Corresponding author*. Tel.: +39 0862 433252.
E-mail address: tofani@di.univaq.it (A. Tofani).
0169-2607/$ – see front matter © 2007 Elsevier Ireland Ltd. All rights reserved.
doi:10.1016/j.cmpb.2007.03.004

1. Introduction

The mechanical function of the heart depends crucially on its material properties. Therefore, according to [1], the objective of the cardiac mechanics research is the understanding of these properties, and how these properties (that relate also to the structure of the tissue) affect the pumping function of the intact heart.

In particular, high passive stiffness is one of the mechanical features that characterize the *cardiac muscle*. There are several studies concerning the components and the architectural aspects of the cardiac muscle responsible for this particular feature [2,3], in particular *cardiomyocytes* and *collagen matrix* have been proposed as candidates.

Cardiomyocyte architecture is widely described in the literature [4,5]; however, many researchers are investigating how the cardiomyocyte architecture is involved in regulating the electrical and mechanical behavior of the cardiac muscle [5,6].

On the other hand, the cardiac collagen matrix is composed by (1) *endomysial collagen* that connects *myocytes* and surrounds, in a mesh-like structure, the myocytes themselves and (2) *perimysial collagen* that groups myocytes together, running in parallel with *myofibrils* and linking itself to endomysial collagen [7–9].

In [9] a mathematical model of perimysial collagen is defined, to describe its role in myocardial mechanics during ventricular filling (*diastolic phase*) and identify the physical parameters characterizing perimysial collagen itself.

On the contrary, the endomysial collagen contribution to passive mechanics of the cardiac muscle is not yet fully understood. In particular, it is still a matter of debate its micro arrangement and how different micro arrangements could influence this mechanics [10,11].

To contribute to this discussion, we propose two computational models to investigate the mechanical and structural properties of endomysial collagen. To this goal, we need simplified computational models of some aspects of the cardiac muscle itself.

We start from the hypothesis that a healthy behavior of the cardiac muscle needs a limited thickness of the microscopical (i.e. endomysial) collagen fibers. This seems to be plausible considering that, as mentioned above, endomysial collagen connects and surrounds the myocytes, so that collagen fibers of excessive thickness could interfere with the normal mechanics of the myocytes themselves (both in the passive and active phase). Moreover, an increase in size of the collagen fibers has been observed in a number of heart disfunctions [7,12]. Finally, the morphological findings of [13,14] (see below) show an arrangement of the endomysial collagen based on very small fibers.

We set up two models:

- The first one is suggested by the mentioned morphological findings described in [13,14], obtained from scanning electron microscopy (SEM) in NaOH macerated samples (see Fig. 1).
- The second one is based on the traditional micro anatomical view of the endomysial collagen reported in [15].

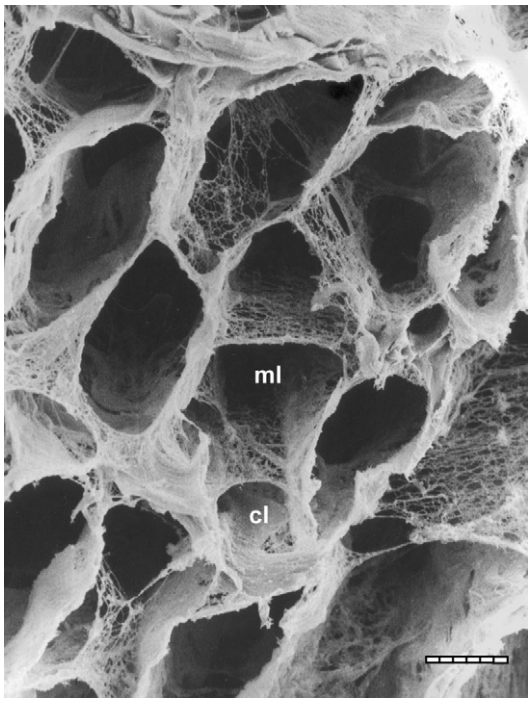

Fig. 1 – The endomysial collagen arrangement (ml: muscular lacunae, cl: capillary lacunae, bar = 10 μm). From [14] with permission.

We model the myocardial tissue as a net of spring elements (in the following simply "springs") representing the cardiomyocytes together with the endomysial collagen distribution. Each element is a viscous elastic spring, characterized by an elastic and a viscous constant. We connect these springs to imitate the interconnections between collagen fibers. Then we apply to the net of springs some external forces of suitable magnitude and direction, obtaining an extension of the net itself. In our setting, the ratio (*forces magnitude*)/(*net extension*) is intended to model the *stress/strain* ratio of a microscopical portion of the myocardial tissue.

Our starting point has been the hypothesis that if the net of springs is structured according to the new point of view of [13,14], then, to obtain a desired *stress/strain* value, in the sense specified above, we need much smaller elasticity constants of the springs than the ones obtained structuring the net according to the traditional point of view [15].

In order to understand whether this is the case, we organize our computational framework in such a way that it is able to *learn* the spring constants corresponding to a specified *stress /strain* value.

Moreover, to analyze the behavior of our nets from the *stress /strain* aspect, we need to consider the equilibrium positions only. Indeed, in the nets of springs that we consider, these equilibrium positions are independent from the viscous constant parameter of the springs (as we also verified by extensive computational experiments). This could be explained by the topology of our nets and the fact that we consider external forces that remain constant during the time period under consideration.

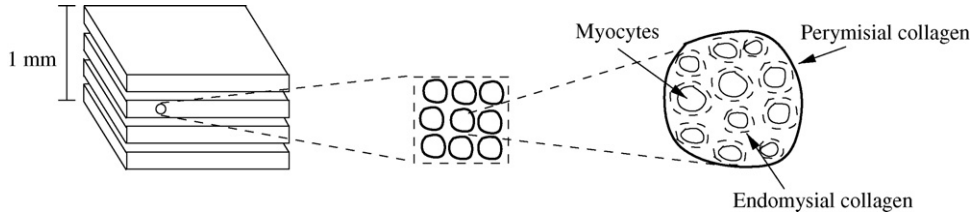

Fig. 2 – The microstructure of the cardiac muscle.

Therefore, in this setting, we do not need to determine the exact values of viscous constants; note, however, that these values would be important in a more complete simulation model (since it is well known that the elastic behavior of the collagen is not linear [16,17]).

To solve the problem of the correct identification of the values of the elastic constants involved, we use an *artificial neural network* approach. In particular, we use this technique to *learn*, given a distribution of external forces, the elastic constants of the springs needed to obtain a desired net extension as an equilibrium position.

To avoid possible misunderstanding observe that:

(1) We always model the myocardial tissue as a net of physical springs.
(2) Artificial neural networks are used only as a computational tool (see below for more details).
(3) That is, we never intend to represent the myocardial tissue as a neural network.

Our computational technique is inspired to the work proposed in [18,19], where pre-structured recurrent artificial neural networks are used to compute the dynamics of viscous-elastic objects represented as spring nets. This technique allows: (1) to avoid to write down (and numerically solve) the entire differential equations system, (2) to learn the main physical parameters determining the spring net and, finally and (3) to model quite different-sized systems, ranging from a micro- to a macro-view of the structures under consideration (i.e., our approach is scalable).

The simulation software can be obtained, under request (see [20]), in order to perform analogous experimentations.

A short preliminary version of our work has appeared in [21]. The present version contains a refined approach, several new experiments and all the details missing in [21].

2. Background

The cardiac tissue is composed of discrete layers of myocardial muscle fibers (called myocardial laminae or sheets [4,1]), as it is shown in Fig. 2. Furthermore, a muscle fiber is composed of heart myocytes and capillaries enmeshed in a net of connective tissue, organized in different levels, as it is shown in Fig. 3:

- *Perimysial collagen* which is associated with groups of myocytes.

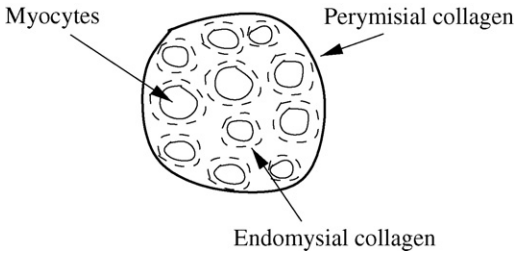

Fig. 3 – The cardiac collagen matrix.

- *Endomysial collagen* which surrounds and connects each individual muscular cell.

Collagen is an essential component of myocardial connective tissue. Collagen arrangement has probably the significance of preserving heart micro-architecture and chamber geometry, maintaining the correct myocyte alignment and possibly contributing to the control of myocardial contraction [13,10,11].

Scanning electron microscopy (SEM) allows the best visualization of the distribution of cardiac endomysial collagen in normal [13,15,14] and NaOH macerated samples (a method for isolating the collagen from other tissues and preserving

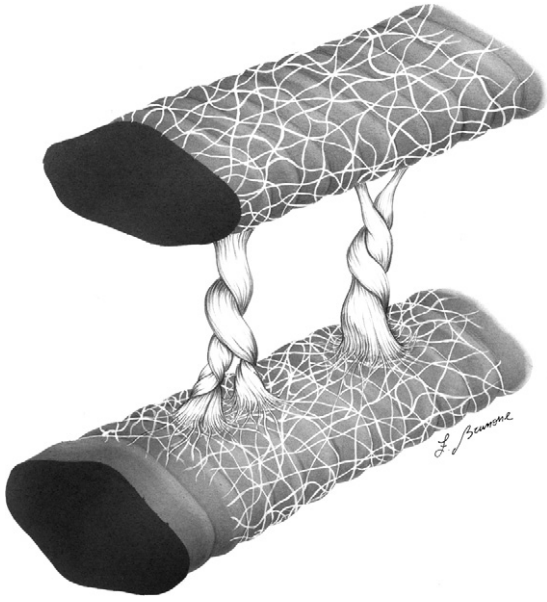

Fig. 4 – Known model of myocardial endomysial collagen distribution. From [13] with permission.

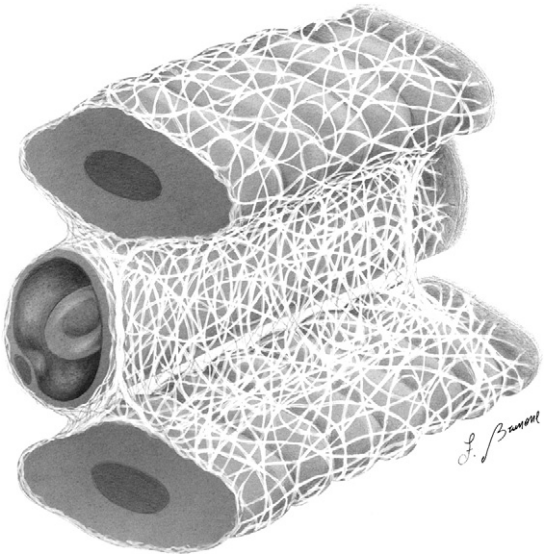

Fig. 5 – Revisited model of myocardial endomysial collagen distribution. From [13] with permission.

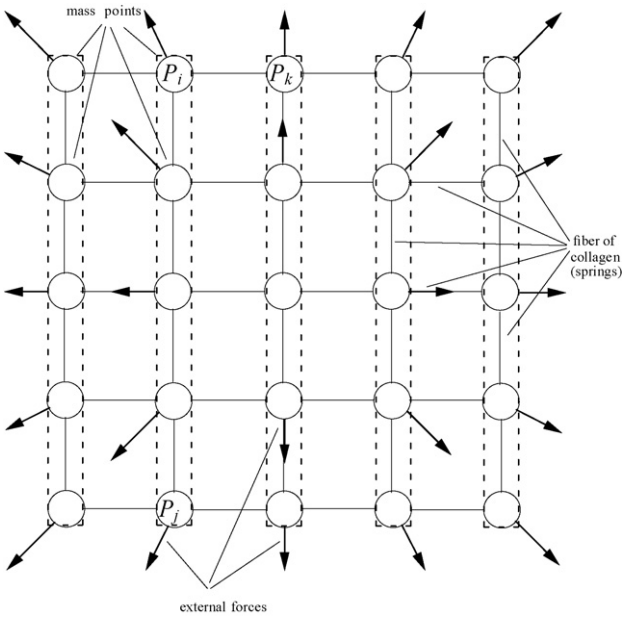

Fig. 6 – The physical model inspired to the view of the distribution of endomysial collagen proposed in [15].

its three dimensional arrangement [13,14]). Fig. 1 has been obtained with this technique.

Fig. 4 shows one view of the endomysial collagen arrangement. It has been described as a weave network surrounding each individual myocyte and connecting adjacent myocytes and capillaries, through bundles of collagen called "struts" [15,7].

Fig. 5 shows another model proposed in [13,14] of myocardial endomysial collagen distribution. The endomysial collagen fibers are organized in a layer enveloping myocytes and capillaries. The endomysial sheath spreads from one myocyte to neighboring ones like a lamina, and extends along the fully myocyte length. This lamina also completely wraps neighboring blood vessels. For more details see [13,14].

To the best of our knowledge, it is still a matter of debate which of the two models of the endomysial collagen microarrangement is to be preferred.

3. Computational technique design

We now illustrate our methodology, by first describing the physical models of myocardial connective tissue that we propose for the collagen arrangements. Then, we illustrate the methodology that we use for our computational experiments.

3.1. *Physical models*

To illustrate the most important features of the proposed physical models, consider Fig. 6. As displayed in the figure, we represent the connective tissue (which is supposed to be made up primarily of collagen [22,13–15]) with a set of connected springs (continuous lines in the Fig. 6), that we call *spring net*. We will refer to the springs application points as *mass points* or *nodes*. The geometrical arrangement of these springs is intended to reflect a specific micro anatomical view of the collagen distribution. Some other springs (those included in the dashed lines in Fig. 6) represent myocytes, which are considered essential elements in developing passive tension [2,23,3].

A value for the elasticity constants of the springs representing myocytes was extrapolated from the Young module of myocytes [3].

Furthermore, from the myocytes dimension and disposition [24] we can (approximately) compute the initial disposition of the mass points. In our work, we have considered two kinds of experimentations (see Section 6) depending on the initial disposition of the vertical mass points:

- In one experimentation, the initial distance between points P_i (the second node in the first row starting from the left) and P_j (the second node in the last row starting from the left) represents the resting length of a myocyte [2,23,24].
- In the other one, the initial distance between points P_i and P_j represents the resting length of a portion of a myocyte (approximatively the length of a sarcomere).

Finally, we suppose that the whole net is stressed by some external forces (the arrows in Fig. 6), which are applied to each mass point. These forces are intended to simulate the stress induced by blood pressure on a microscopic piece of myocardial tissue. As a matter of fact, during the diastolic phase the whole cardiac muscle is enlarged. If we consider this dilatation on a microscopic portion of the cardiac muscle, we can suppose that the stress acts in all directions; thus, the vectors representing the forces are initialized in such a way to locally reflect this assumption (Fig. 6). Namely, we set the forces direction to be radial w.r.t. the center of the spring net. The magnitude of this vector is approximated starting from the mean value of diastolic pressure and it is comparable with values in the literature [24], regarding the passive strength on sarcomeres during diastole.

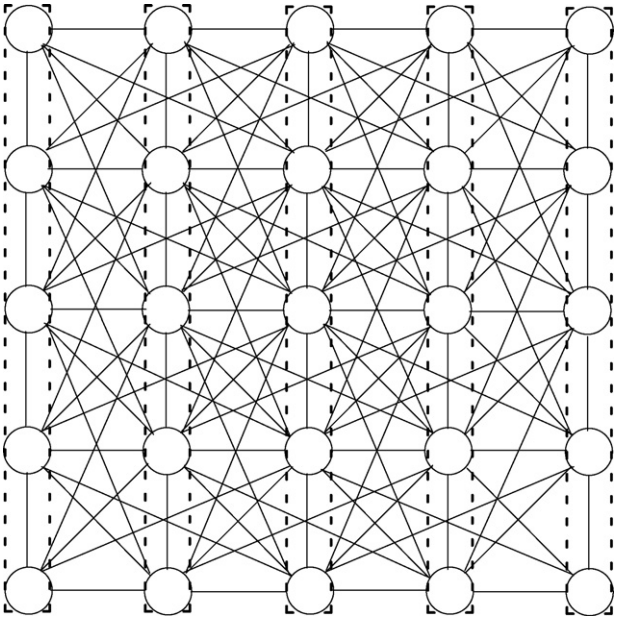

Fig. 7 – The physical model inspired to the view of the distribution of endomysial collagen proposed in [13].

In order to investigate the differences between the model inspired to the micro arrangement view of Fig. 4 as opposed to the model inspired to the view proposed in Fig. 5, we will use the physical models shown in Fig. 6 and 7, respectively.

The physical model in Fig. 6 is based on the micro arrangement showed in Fig. 4: in fact, there are few connections and only between adjacent myocytes. On the contrary in Fig. 7, which is based on Fig. 5, we have that each mass point is connected in a more complex way to the other mass points. The connections are such that all the mass points which are sufficiently close are connected.

So we introduce the following definitions:

Definition 1 (Simple Net). We call *Simple Net* a net such that nodes (i.e. mass points) are connected only with adjacent nodes along horizontal lines and vertical lines (see Fig. 6).

Definition 2 (Complex Net). We call *Complex Net* a net where the connections are such that all the nodes (i.e. mass points) which are sufficiently close are connected (see Fig. 7).

In our computational experiments we have considered Simple/Complex Nets with different numbers of mass points (see Section 6).

Fig. 8 summarizes our proposed models.

Note that, a *bias* is induced by the particular square-like net topologies used. Indeed, since there are mass points which are more interconnected, they receive a stronger stress. This bias could be avoided by more symmetrical topologies (e.g. cylindrical ones). However, we use square-like topologies (which are simpler from the computational point of view) since the bias remains the same both in the Simple and Complex Nets,

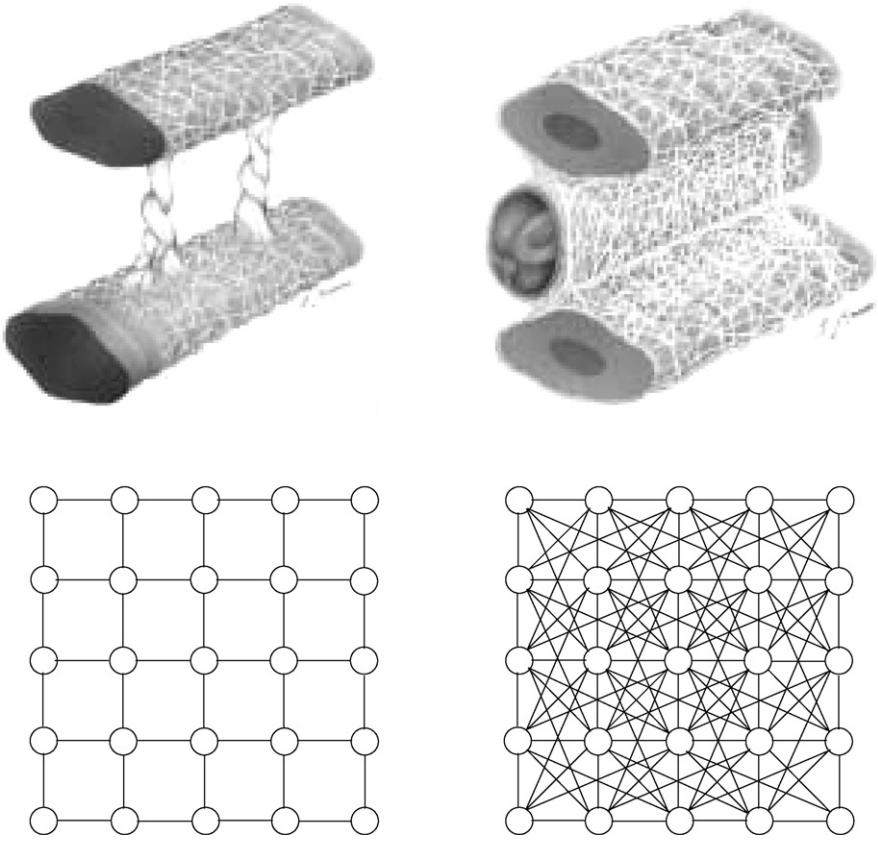

Fig. 8 – The micro-anatomical views of endomysial collagen distribution and the corresponding physical models.

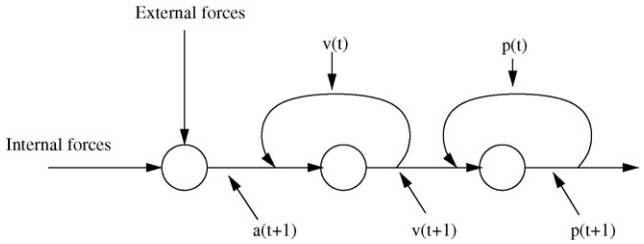

Fig. 9 – A mass point module.

so that the comparison between the two kinds of nets is not substantially affected.

3.2. *The computational model*

We use artificial neural networks to compute the dynamics of our spring nets. Note that, in a conventional approach, a system of differential equations must be constructed for each spring net. Depending on the complexity of the net, the construction of the differential equations system could be extremely cumbersome; moreover, the identification of the right parameters [18,19] and the numerical computation of solutions could be very complex.

Our use of artificial neural networks is inspired to [18,19]. More in detail, in [18,19] two distinct neural computational units (called *modules*) are used, each computing the dynamics of a particular element of the physical model. The first module (*mass point module*) is composed by neurons that compute the dynamics of the mass points, whereas the second module (*spring module*) is composed by neurons that compute the dynamics of the springs.

These modules are connected together according to the physical model. The resulting neural network is *recurrent*, since there are self-connected neurons (called integrator units, see [18]).

More in detail, the mass point module consists of three distinct neurons as shown in Fig. 9. These neurons compute respectively the *acceleration*, the *velocity* and the *position* of each mass point.

On the other hand, the spring module (Fig. 10) computes the instantaneous reaction force engendered by a stressed spring. This force depends on the position and the velocity of the uttermost points of the spring. Note that, in Fig. 10, the weights of the connections to the neuron that computes the instantaneous reaction force (neuron F in Fig. 10) represent the constants characterizing the spring: the elastic (k in Fig. 10) and the viscous one (v in Fig. 10); the viscous constant is required to be greater than zero in order to stop at an equilibrium position.

3.3. *The learning procedure*

Our goal is to learn, given a distribution of external forces, suitable values for the elastic constants of the springs needed to obtain a desired net extension (that is, in our setting, the net *strain*) as an equilibrium position.

More in detail, our algorithm takes as an input a desired net strain (both vertical and horizontal), which is defined w.r.t. the geometric center of the net itself. Then, the net is stressed by given external forces; this input is propagated on the net, and all the mass points positions are recomputed accordingly. Since we use viscous-elastic springs, this *propagation procedure* will stop when the net reaches an equilibrium position. Since we are interested only in these equilibrium positions, we use springs with an arbitrary viscous parameter value; indeed, as we mentioned in Section 1, the equilibrium positions are independent from the value chosen for the viscous parameter. This could be explained by the topology of our nets and the fact that we consider external forces that remain constant during the time period under consideration. We have verified this property by extensive computational experiments.

If the computed equilibrium position is not sufficiently close to the given target position, then the elastic constants of the springs are updated (see below) and the propagation procedure is restarted (according to the usual neural network terminology [25], this step is called a *learning era*). When the equilibrium position is sufficiently close to the target position, the learning process is completed.

The most crucial step of our learning algorithm is the update of the elastic constants of the springs . To cope with this problem, we adopt a particular updating method different from those suggested in the literature [25,18,19]. In the following, we illustrate our updating procedure.

Suppose we are given n springs. The global error modulus at the end of the propagation procedure is computed as follows:

$$E = \max_{1\le i\le n} |E_i| \tag{1}$$

being, for all $i = 1, \ldots, n$

$$E_i = \frac{d_i - a_i}{a_i} \tag{2}$$

where a_i is the actual length and d_i is the desired length of the spring i; recall that we compute the desired length of each spring i depending on the vertical/horizontal strain imposed to our net (see Section 6).

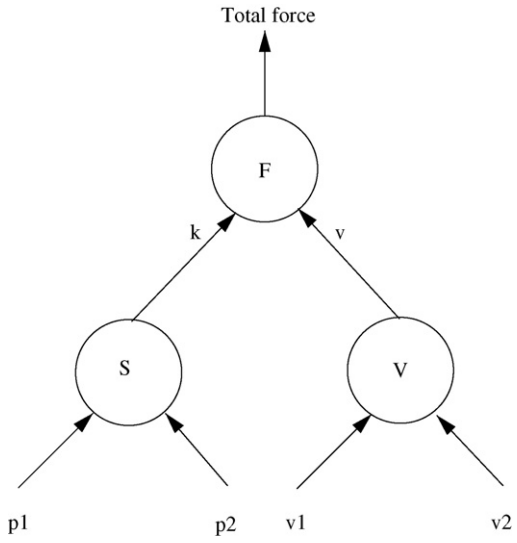

Fig. 10 – A spring module.

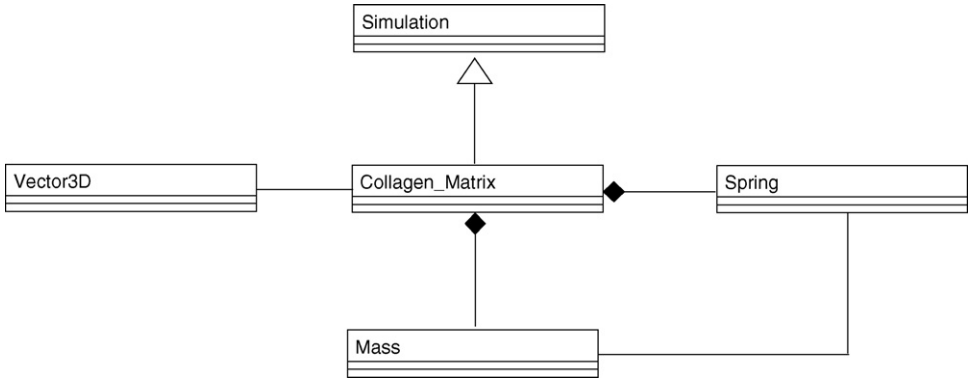

Fig. 11 – The computational technique architecture.

If the global error modulus E is less or equal to a given tolerance then the learning procedure terminates, otherwise we update the elastic constant (k_e_i) of the springs in the following way:

$$k'\_e_i = k\_e_i + \mu E_i k\_e_i \quad (3)$$

where $\mu \in [0, 1]$ is a constant that regulates the update velocity and it is used in order to prevent the overshooting problem [25,19]. In our experiments we have used $\mu = 1/2$. Our experiments show that our update rule is able to reduce the global error and that the termination of our learning procedure is independent from the springs update order.

4. System description

Our computational technique is based on a special purpose C++ implementation of the physical simulation engine of [26]. The source code with a detailed documentation can be found in [20]. Our tool is composed of a math library, a simulation engine and a procedure that realizes the specific physical simulation. In particular:

- The math library is included in a class named Vector 3D used in order to represent points and vectors in three dimensional space. This class allows to represent: the position, the velocity, the acceleration and the forces acting on every mass point of the net, as well as the force engendered by each spring.
- The simulation engine allows to manage the simulation procedure of our physical models (i.e. the motion of the mass points and the springs behavior).
- The application uses the simulation engine and the math library in order to implement the specific physical simulation.

The simulation engine comprises the following classes:

- The *class simulation*, that implements the simulation steps.
  - [
  - bullet] It computes the internal forces using the class spring (see below).
  - [
  - bullet] It applies the external forces.
  - [
  - bullet] It computes the new positions and new velocities of the mass points using the class mass (see below).
- The *class mass* that implements the mass point module (see Section 3.2). The module, representing the mass point dynamics consists of three distinct neurons as shown in Fig. 9. These neurons compute respectively the *a* cceleration, the *velocity* and the *position* of each mass point (method *simulate* ()).
- The *class Spring* that implements the spring module (see Section 3.2). The spring module (Fig. 10) computes the instantaneous reaction force engendered by a stressed spring (method *solve* ()). The reaction force depends on the position and the velocity of the uttermost points of the spring.

Fig. 11 shows the overall class architecture. We have omitted the detailed description of class variables and methods, since they are available at [20].

The class *Collagen_Matrix* of Fig. 11 implements the overall computational technique. It extends the simulation class, and it is used to set up the environment and to implement the methods of the learning procedure described in Section 3.3. The main methods of the *Collagen_Matrix* class can be summarized as follows:

- *Propagate* (). The system is stressed by the external forces; this input is propagated on the net, and all the mass points positions are recomputed accordingly. This propagation procedure stops only when the net reaches an equilibrium position (see Section 3.3).
- *Update* (). This method updates all the elastic constants of the springs, in order to reduce the global error. It computes these constants according to the updating rule (3) of Section 3.3.
- *Learning* (). This method implements the learning algorithm of Section 3.3 and it returns the learning eras.

Furthermore, the *Collagen_Matrix* class implements auxiliary methods in order to initialize the physical model depending on the user choices (i.e. Complex or Simple Net, the initial geometrical dimensions and numerical settings).

```
1. Acquire initial parameters, both geometrical and physical;
2. Acquire the target final positions;
   begin (Learning)
   2.1 Initialize the computational model;
   2.2 Acquire external forces;
       begin (Propagation)
       2.2.1 Compute the internal forces acting on each mass point;
       2.2.2 Compute the new positions of the mass points (by
             applying the already computed internal forces);
       2.2.3 Propagate the results of step 2.2.2;
       2.2.4 If equilibrium is reached then stop propagation,
             else go to 2.2.1;
       end(Propagation)
   2.3 Compute the error between the actual final positions and
       the target final positions;
   2.4 If the error is less than or equal to a given tolerance
       then stop Learning;
   2.5 Otherwise, update the springs elastic constants
       and go to 2.1;
   end (Learning)
```

Fig. 12 – *Collagen_Matrix* control flow.

Fig. 12 shows a concise description of the *Collagen_Matrix* control flow.

5. Status report

The implementation of the proposed computational technique, available at [20], is a preliminary version of a tool that, by a proper *graphical user interface* and an *empowered parallel simulation engine*, might allow the simulation of the myocardial tissue dynamics. Furthermore, it might allow the experimentation of the influences, on the myocardial tissue dynamics, of different morphological and micro architectural arrangements of the microscopic components of the myocardial tissue itself.

Also the preliminary version of our tool shows a substantial easy of use, in particular:

- It is possible to easily change the experiment parameters.
- It allows an easy rearrangement of the net topology.

Furthermore, we are working on a parallel version of the algorithm that will allow us to experiment with net systems composed of thousands of springs. This could be used to simulate more significant portions of the cardiac muscle (e.g. the whole structure of the muscular fibers). See Section 7 for an evaluation of the computational complexity needed for these tasks.

The implementation of the parallel version is based on the *message passing interface* [27] and we already started to test it on a parallel computer with a 64 node cluster.

In Section 6 we show the experimental results that we obtained with the present version of the tool and we report some of its time performances (Table 9).

6. Experimental results

Finally, we present our experimental results. As mentioned above (see Section 3.1), we have carried out two kinds of experimentations: one on a *small scale*, the other on a *large scale* setting.

6.1. Experimental settings

The experimentations that we have carried out depend on various parameters.

6.1.1. Geometrical dimensions

Here we deal with the dimensions of myocytes and the distances between them. In order to reflect the real myocytes arrangement (as it can be found in the literature [13,14,2,23,24]):

- In the *small scale experimentation* we set the distance between two vertical mass points (see Figs. 6 and 7) to 1.6 μm, that is the resting sarcomere length for human myocytes.
- In the *large scale experimentation* we set the distance between two vertical mass points (see Figs. 6 and 7) to 15 μm, to obtain a vertical length of the net comparable to the length of a human myocyte.

In both experimentations the distance between two parallel myocytes is estimated to 15 μm [13].

6.1.2. Physical parameters

Here we deal with physical parameters of the springs and of the environment. They are embedded in: *external forces* magnitude and direction, *desired net strain*, *initial elastic constant* and *viscous constant*. As already said, external forces of the same magnitude are applied on each mass point and have a radial direction (see Fig. 6). Moreover, their magnitude is calculated from the mean value of the end diastolic pressure (about 20 mmHg) and by considering the area of the net.

In order to choose the desired net strain parameter we consider both the vertical and the horizontal strain. For the vertical strain, in our experimentations we use values ranging from 20% to 35%. This range is consistent with the values which can be found in the literature (e.g. [13]).

On the other hand, the horizontal strain is chosen in the range between 0% and 2%. In fact, we suppose that in the desired final disposition the myocytes will be only slightly spaced out.

Finally, the initial elastic constants are chosen (by trials) in a way such that the initial strain is not too far from the desired net strain, while the viscous constant is chosen (by trials) to reduce the number of iterations required to obtain an equilibrium state.

6.1.3. Net management

Here we deal with tolerances, namely the *propagation tolerance* and the *learning tolerance*. The propagation tolerance regulates the equilibrium state trapping. Indeed, we say that the net is in a equilibrium state when the resulting forces on all of the mass points are *sufficiently near to zero* in magnitude.

The learning tolerance is used in order to decide the termination of learning algorithm. Namely, the error as defined in Eq. (1) of the Section 3.3 has to be less or equal to the learning tolerance in order to stop the learning process.

We have chosen a value for the learning tolerance (i.e. 10^{-3}) in such a way that the final mass points positions are quite equivalent to the desired ones. Therefore, we need a great

Table 1 – System parameters

Geometrical and physical parameters	
Myocyte diameter	15 μm
External force	5.0^{-6} N
Viscous constant	2.0^{-3} kg s^{-1}
Small scale experimentation	
Sarcomere initial length	1.6 μm
Sarcomere final length	1.92, 2.0, 2.2 μm
Initial k_e for *Simple Net*	10.0
Initial k_e for *Complex Net*	1.0
Large scale experimentation	
Sarcomere initial length	15 μm
Sarcomere final length	18, 18.75, 20.25 μm
Initial k_e for *Simple Net*	100.0
Initial k_e for *Complex Net*	1.0
Numerical parameters	
Propagation tolerance	10^{-10}
Learning tolerance	10^{-3}

number of learning eras in order to obtain the desired net behavior.

6.1.4. *Numerical results*

In order to compare the experimental results of different nets of springs based on different micro-arrangements of endomysial collagen and different scale experimentations, we focused on several numerical results:

- The mean value of the springs elasticity constants (MVSEC).
- The ranges of such constants.
- The standard deviations.

The MVSEC comparison allows to investigate whether the net of springs structured according to the point of view of [13,14], obtains a desired *stress/strain* ratio with much smaller elastic constants than the ones obtained structuring the net according to the traditional point of view [15] (see Section 1). The other numerical results are used to compare the resulting elastic constants distribution of the different nets of springs.

The values for all the experimental parameters are summarized in Table 1.

6.2. *Experiments*

As we mentioned before, we have carried out a small and a large scale experimentation. For each scale, we have considered Simple/Complex Nets with different numbers of rows and columns of nodes (see Fig. 7) in order to demonstrate the independence of our results from the dimension of our physical models. Our experimental results are summarized in Tables 2 and 3 for the small scale experimentation, in Tables 4 and 5 for the large scale experimentation.

Our experimental results show that the Complex Nets obtain a desired *stress /strain* ratio with much smaller elastic constants than the ones obtained with Simple Nets. In particular, in the large scale experimentation (see Tables 4 and 5) the Complex Net MVSEC, defined in Section 6.1, is two order of magnitude smaller than the Simple Net one. For example, consider the first raw of the Table 5; we have the pair 20%, 0% for the desired pair of vertical, horizontal strain. In this case,

Table 2 – Small scale experimentation; grid of dimension 12×6, with 126 springs in the *simple* case and 424 in the *complex* case

Strain (%)		Net MVSEC	
Vertical	Horizontal	Simple	Complex
20	0	173.25	12.25
25	0	172.13	10.29
35	0	170.85	7.47
20	1	20.87	3.61
25	1	19.75	3.21
35	1	18.46	2.68
20	2	13.63	2.63
25	2	12.50	2.30
35	2	11.22	1.90

Table 3 – Small scale experimentation; grid of dimension 10×10, with 180 springs in the *simple* case and 630 in the *complex* case

Strain (%)		Net MVSEC	
Vertical	Horizontal	Simple	Complex
20	0	462.554947	56.885567
25	0	461.604191	46.349658
35	0	460.518627	34.615436
20	1	46.384052	6.401356
25	1	45.433484	5.989074
35	1	44.347190	5.377360
20	2	26.553699	3.821141
25	2	25.603186	3.579189
35	2	24.516804	3.241656

we obtain a value for the Simple Net MVSEC of 356.29, whereas the Complex Net MVSEC is 1.45.

A natural question is whether the reduction of the values of the elastic constants is caused simply by the increase of the number of the springs. To show that this is not the case, we consider the *MVSEC reduction factor*, defined as the ratio: (*Simple Net MVSEC*)/(*Complex Net MVSEC*), of the small and large scale experimentation, w.r.t. the springs number increase defined as the ratio of the Complex Net springs number w.r.t. the Simple Net springs number. In Table 6 we consider the *MVSEC*

Table 4 – Large scale experimentation; grid of dimension 12×6, with 126 springs in the *simple* case and 424 in the *complex* case

Strain (%)		Net MVSEC	
Vertical	Horizontal	Simple	Complex
20	0	168.490759	0.542115
25	0	168.347853	0.459164
35	0	167.768512	0.332462
20	1	17.665179	0.532107
25	1	17.153658	0.432824
35	1	16.574341	0.317041
20	2	10.460759	0.502985
25	2	9.955909	0.411574
35	2	9.373616	0.303957

Table 5 – Large scale experimentation; grid of dimension 10×10, with 180 springs in the *simple* case and 630 in the *complex* case

Strain (%)		Net MVSEC	
Vertical	Horizontal	Simple	Complex
20	0	356.293965	1.457676
25	0	355.941777	1.228320
35	0	355.539922	0.993332
20	1	33.996654	1.117011
25	1	33.644452	0.963810
35	1	33.242577	0.787278
20	2	18.647347	0.930340
25	2	18.295137	0.814883
35	2	17.893247	0.674460

reduction factor of the Simple Net w.r.t. the Complex Net of grid dimension 10×10, for both the small and large scale experimentation, as it can be deduced from Tables 3 and 5, respectively. The Table shows that the MVSEC reduction does not depend only on the number of springs but also on the *net topology*, e.g. in the first row, the number of springs has increased of a 3.5 factor, whilst the MVSEC has been reduced, in the large scale experimentation, of a factor near to 246, so that there is a "gain" of approximatively a factor 242.5 due to the net topology.

Tables 7 and 8 show, w.r.t. the small and, respectively, the large settings, the elastic constants ranges and the elastic constants standard deviations—obtained with the net of grid dimension 10×10. The high values obtained, in both cases, for the Simple Net, are due to the fact, discussed above, that some springs are much more stressed than the others. This also happens in the Complex Net case, but the net topology helps in distributing the stresses. This is a further aspect for considering the Complex Nets more adequate. Nevertheless, the distribution of the stresses seems to be a complex task, as illustrated in the Fig. 13 which still refers to a Complex Net of grid dimension 10×10; indeed, this figure shows that – in the small scale experimentation – most springs (91.11%) have a small value for the elastic constant, and a few springs (1% approximatively) have very big values. This can be explained by considering that the *required* horizontal strain is very small, so that the horizontal springs have to ensure this, getting big elastic constants. (On the other hand, from a morphological point of view, the presence of collagen fibers of very different sizes, seems to be expected from the kind of *fractal* structure displayed in Fig. 1).

Finally, Table 9 reports the time performances of the current implementation for the small scale experimentation and large scale experimentation of a particular net system that we consider as a benchmark. In particular, we have considered the time performances w.r.t. a Complex Net where we imposed a 25% of vertical strain and 0.01% of horizontal strain.

Table 6 – Comparison of the simple/complex net reduction factor w.r.t. complex/simple net springs number increase

Strain (%)		MVSEC reduction factor		Springs number increase factor
Vertical	Horizontal	Small scale exp.	Large scale exp.	
20	0	8.1	245.7	3.5
25	0	9.9	291.7	3.5
35	0	13.3	359.1	3.5
20	1	7.2	30.6	3.5
25	1	7.5	35.0	3.5
35	1	8.2	42.6	3.5
20	2	6.9	20.0	3.5
25	2	7.1	22.5	3.5
35	2	7.5	26.7	3.5

Net grid dimension: 10×10 nodes.

Table 7 – Small scale experimentation; grid of dimension 10×10; elastic constants ranges and the elastic constants standard deviations

Strain (%)		Elastic constants range				S.D.	
Vertical	Horizontal	Simple		Complex		Simple	Complex
		Min	Max	Min	Max		
20	0	1.6	1662.9	0.0	414.0	544.0	53.0
25	0	1.3	1662.9	0.0	344.6	544.8	45.8
35	0	0.9	1662.9	0.0	286.3	545.7	40.1
20	1	1.6	151.2	0.0	20.4	46.3	3.8
25	1	1.3	151.2	0.0	16.0	46.9	3.6
35	1	0.9	151.2	0.0	16.1	47.7	3.3
20	2	1.6	79.1	0.0	22.3	23.0	2.7
25	2	1.3	79.1	0.0	17.0	23.5	2.3
35	2	0.9	79.1	0.0	10.9	24.1	2.0

Table 8 – Large scale experimentation; grid of dimension 10 × 10; elastic constants ranges and elastic constants standard deviations

Strain (%)		Elastic constants range				S.D.	
Vertical	Horizontal	Simple		Complex		Simple	Complex
		Min	Max	Min	Max		
20	0	0.9	1538.7	0.007	12.9	420.1	2.0
25	0	0.7	1538.7	0.004	12.1	420.4	1.8
35	0	0.5	1538.8	0.001	12.4	420.7	1.7
20	1	0.9	139.8	0.01	8.0	36.9	1.3
25	1	0.7	139.8	0.005	8.8	37.1	1.2
35	1	0.5	139.9	0.002	8.0	37.5	1.2
20	2	0.9	73.2	0.01	5.8	18.6	1.0
25	2	0.7	73.2	0.007	5.8	18.9	0.9
35	2	0.5	73.2	0.002	6.0	19.2	0.9

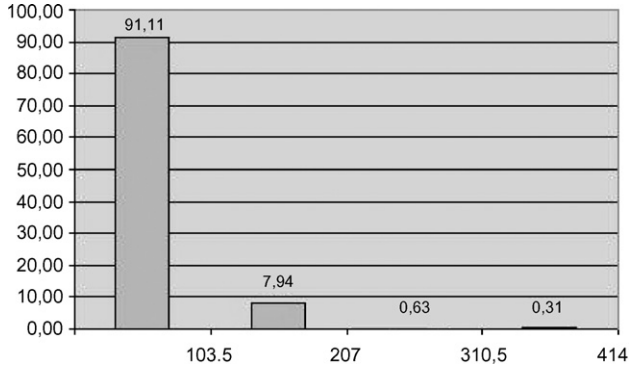

Fig. 13 – Distribution of the elastic constants in a Complex Net of grid dimension 10 × 10.

Table 9 – Computational technique time performances

Grid dimension	Small scale exp. (s)	Large scale exp. (s)
10 × 10	2739	576
12 × 6	241	260

The experimental results were obtained on a machine with four processors (all Intel Xeon 2.80 GHz) and 4 GB of RAM.

It is clear that with this computational technique we are not able to cope with nets of thousand nodes. So, as discussed in Section 5 and in Section 7, we are considering a *parallel version* of the algorithm.

7. Discussion

In this work we have proposed a computational technique that could be used to model and simulate the mechanics of a microscopical portion of myocardial tissue.

Indeed, it is very likely that suitable arrangements of nets of (possibly non linear) springs are able to physically simulate any kind of elastic behavior of soft tissues. Two points are to be stressed:

(1) We do not claim, in any way, that the modelling problem is thus automatically solved; indeed, even assuming that we are able to treat – from a computational point of view – very large nets and even several connected large nets (e.g. to simulate the interconnections between the myocardial sheets, see Fig. 2), the structure of each net as well as the interconnections between the different nets have to be specified in a meaningful way.
(2) The neural network technology can be of great help to cope with the computational complexity involved in simulations based on spring nets, in particular, for the parameters determination problem and for experimentations concerning the structural arrangement.

The current implementation of our computational technique is a preliminary version, but it has interesting characteristics.

First of all, it was possible to obtain some stimulating computational results. Actually, if we consider Tables 7 and 8, it could be noted that the elastic constants values computed for the Complex Net are consistent with the physiological dimension of the endomysial collagen (see Fig. 1).

Indeed, consider the maximum values of the elastic constant for the Simple Net and the Complex Net of Table 8, that we denote with M^k_{SN} and M^k_{CN} respectively. From Eq. (4) below (where E, A, L and k denote – w.r.t. a collagen fiber sample – the Young modulus, the cross sectional area, the length and, respectively, the elastic constant), it could be computed the cross-sectional area A of a collagen fiber sample of length $L = 10\,\mu$ m (approximately the length of the springs in our nets for the large scale experimentation) and Young modulus $E = 1$ Gpa [17]:

$$E = \frac{k \times L}{A} \tag{4}$$

In particular, using the M^k_{SN} values, we obtain a cross-sectional area of the collagen fiber of the same order of magnitude of the cross-sectional area of a myocardial fiber, whilst, using the M^k_{CN} values, we obtain a cross-sectional area of a order of magnitude comparable with the physiological dimension of endomysial collagen fibers. This result is in agreement with the morphological findings described in [13,14] (see also Fig. 1).

Moreover, our computational technique is scalable w.r.t. the number of springs and nodes. In particular, we want to

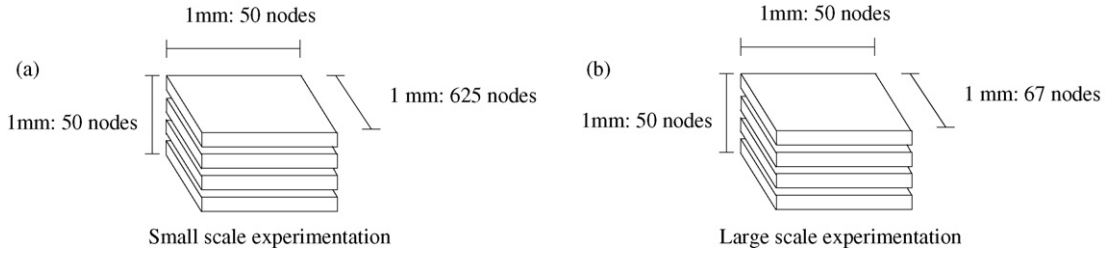

Fig. 14 – An example of a more complex model.

make use of nets with a very large number of nodes (and springs), in order to construct approximate models of a portion of cardiac tissue of a few millimeters.

Furthermore, we can try to computationally reconstruct the model of perimysial collagen considered in [9]. Since this model is based on differential equations related to a mechanical model of perimysial collagen fibers, it will be of interest to obtain similar results making use of computational elements representing the myocardial tissue at a lower scale. Moreover, we can also consider the contribution of the endomysial collagen.

In these new settings, we have to deal with a huge demand of computational resources. As an example, consider a cube-shaped portion of myocardial tissue with 1mm edges as shown in Fig. 14. Consider the following settings:

- A myocyte is length 80 μm and its diameter is 20 μm [1].
- A myocardial sheet is five myocytes thick [1,5].
- To model a myocyte we need (approximatively) 625 (67) nodes in the small (respectively large) experimentation setting (see Section 6.1).
- Then, to model a myocardial sheet we need (approximatively) 160,000 (17,000) nodes in the small (respectively large) experimentation setting.

Therefore, we need approximatively of 1,600,000 (170,000) nodes in the small (respectively large) scale experimentation setting to model the cube-shaped portion of myocardial tissue shown in Fig. 14. The resulting computation is clearly untractable, for both the experimentation settings, by a traditional desktop machine. To cope with this problem, we are experimenting a parallel version of our computational technique that allows to distribute the computation on a processor cluster. In particular, the parallel version implementation is based on the *message passing interface* [27] and we already started the experimentation on a parallel computer with a 64 node cluster. Moreover, we are planning to exploit the *Condor* [28] high-throughput computing environment in order to further scale up our models.

To conclude, the proposed computational technique could be a useful experimentation framework to model and simulate different aspects of a microscopic portion of the cardiac tissue. Moreover, our computational technique could be considered a bottom-up approach to the experimentation of some mechanical properties of the cardiac tissue, which results could be integrated with the results obtained by other computational techniques, mainly focussed on *finite element methods* [1,29].

8. Conclusion and future work

Our experimental results seem to indicate that, by an appropriate structure, a given *stiffness* (i.e. *stress /strain* ratio) of the myocardial tissue can be obtained with endomysial collagen fibers of much smaller size. Moreover, as already noticed, our results are consistent with the ones in [4]. We also hope that the possibility that larger collagen fibers do not necessarily give a greater stiffness could help to explain some problems exposed in [7]. Indeed, this paper pointed out that an higher density of fibrils collagen does not always imply a greater myocardial and ventricular stiffness. So, it is the collagen structure (e.g. arrangement and distribution) and not only the collagen density to be relevant (see also [9]).

There are two natural directions for extending the present work.

First of all, we plan to model also the systolic phase and make computational experiments similar to those performed for the diastolic phase. In the systolic phase, the models will be more complex since we have to take into account also the myocytes contraction.

Moreover, as discussed in the previous Section, we want to make use of nets with a large number of springs and nodes, so that they can be used to construct approximate models of a portion of cardiac tissue of a few millimeters.

More in general, we hope that our approach can be extended to a bottom-up analysis of the myocardial mechanics, which can complement the top-down approach of [1,29].

Acknowledgement

We thank the anonymous referees for their help in improving a previous version of the paper.

REFERENCES

[1] M. Nash, P. Hunter, Computational mechanics of the heart-from tissue structure to ventricular function, J. Elast. 61 (2001) 113–141.
[2] A. Brady, Length dependence of passive stiffness in single cardiac myocytes, Am. J. Physiol. 260 (1991) H1062–H1071.
[3] D. Fish, J. Orenstein, S. Bloom, Passive stiffness of isolated cardiac and skeletal myocytes in the hamster, Circulation 54 (3) (1984) 267–276.

[4] K.D. Costa, Y. Takayama, A.D. McCulloch, J.W. Covell, Laminar fiber architecture and three-dimensional systolic mechanics in canine ventricular myocardium, Am. J. Physiol. 276 (1999) H595–H607.
[5] I. LeGrice, B. Smaill, L. Chai, S. Edgar, J. Gavin, P. Hunter, Laminar structure of the heart: ventricular myocyte arrangement and connective tissue architecture in the dog, Am. J. Physiol. 269 (1995) H571–H582.
[6] I. LeGrice, B. Smaill, D. Hooks, A. Pullan, B. Caldwell, P. Hunter, Cardiac structure and electrical activation: models and measurement, Proc. Aust. Physiol. Pharmacol. Soc. 34 (2004) 141–149.
[7] J.S. Janicki, B.G.L. Brower, The role of myocardial fibrillar collagen in ventricular remodeling and function, J. Card. Fail. 8 (6) (2002) S319–S325.
[8] B. Burlew, K.T. Weber, Connective tissue and the heart. Functional significance and regulatory mechanisms, Cardiol. Clin. 18 (3) (Aug 2000) 435–442.
[9] D. MacKenna, S. Vaplon, A. McCulloch, Microstructural model of perimysial collagen fibers for resting myocardial mechanics during ventricular filling, Am. J. Physiol. 273 (1997) H1576–H1586.
[10] L.A. Taber, G.I. Zahalak, Theoretical model for myocardial trabeculation, Develop. Dyn. 220 (2001) 226–237.
[11] P.P. Purslow, The structure and functional significance of variations in the connective tissue within muscle, Compar. Biochem. Physiol. A 133 (2002) 947–966.
[12] J. Omens, D. Milkes, J. Covell, Effects of pressure overload on the passive mechanics of the rat left ventricle, Ann. Biomed. Eng. 23 (1995) 152–163.
[13] G. Macchiarelli, O. Ohtani, S. Nottola, T. Stallone, A. Camboni, I. Prado, P. Motta, A micro-anatomical model of the distribution of myocardial endomysial collagen, Histol. Histopathol. 17 (2002) 699–706.
[14] G. Macchiarelli, O. Ohtani, Endomysium in heart left ventricle as showed by sem-naoh maceration method, Heart 86 (2001) 416.
[15] T. Robinson, L. Cohen-Gould, S. Factor, Skeletal framework of mammalian heart muscle. arrangement of inter and pericellular connective tissue structures, Lab. Invest. 49 (1983) 482–498.
[16] J.D. Humphrey, Cardiovascular Solid Mechanics: Cells, Tissues, and Organs, Springer Verlag, 2002.
[17] Y.C. Fung, Biomechanics: Mechanical Properties of Living Tissues, Springer Verlag, 1993.
[18] A. Nürnberger, A. Radetzky, R. Kruse, A problem specific recurrent neural network for the description and simulation of dynamic spring models, in: Proceedings of the International Joint Conference on Neural Networks, Anchorage, AK, 1998, pp. 468–473.
[19] A. Nürnberger, A. Radetzky, R. Kruse, Using recurrent neuro-fuzzy techniques for the identification and simulation of dynamic systems, Neurocomputing 36 (1–4) (2001) 123–147.
[20] http://www.di.univaq.it/tofani.
[21] B. Intrigila, G. Macchiarelli, I. Melatti, A. Tofani, Computational models of the micro architecture of cardiac endomysial collagen, in: C.R. Jiri Hozman, P. Kneppo (Eds.), IFMBE Proceedings of the Third European Medical, Biological Engineering Conference, EMBEC05, vol. 11, Prague, IFMBE, 2005, ISSN 1727-1983.
[22] A.V. Hill, The heat of shortening and dynamic constants of muscle, Proc. R. Soc. London Ser. B. Biol. Sci. 126 (1938) 136–195.
[23] A.J. Brady, Mechanical properties of isolated cardiac myocytes, Physiol. Rev. 71 (1991) 413–428.
[24] M.R. Zile, K. Richardson, M.K. Cowles, J.M. Buckley, M. Koide, B.A. Cowles, V. Gharpuary, G. Cooper, Constitutive properties of adult mammalian cardiac muscle cells, Circulation 98 (1998) 567–579.
[25] J. Hertz, A. Krogh, R. Palmer, Introduction to the Theory of Neural Computation, Addison-Wesley Publishing Company, Inc., Redwood City, CA, 1991.
[26] http://nehe.gamedev.net/data/lessons/lessons.asp?lesson=39.
[27] E.L.W. Gropp, A. Skjellum, Using MPI, 2nd Edition: Portable Parallel Programming with the Message Passing Interface, MIT Press, 1994.
[28] http://www.cs.wisc.edu/condor/.
[29] H. Schmid, M. Nash, C. Walker, G. Sands, A. Pope, I. LeGrice, A. Young, P. Nielsen, P. Hunter, A framework for multi-scale modelling of the myocardium, in: C.R. Jiri Hozman, P. Kneppo (Eds.), IFMBE Proceedings of the Third European Medical, Biological Engineering Conference, EMBEC05, vol. 11, Prague, IFMBE, 2005, ISSN 1727-1983.